Computational Mechanics
https://doi.org/10.1007/s00466-023-02421-9

ORIGINAL PAPER

A digital-twin and rapid optimization framework for optical design of indoor farming systems

Emre Mengi[1] · Carla J. Becker[1] · Mostafa Sedky[1] · Shao-Yi Yu[1] · Tarek I. Zohdi[1]

Received: 8 August 2023 / Accepted: 2 November 2023

Abstract
In the face of a changing climate and a rising number of “food deserts" in both rural and urban areas, there is a demand to supply fresh produce year-round to communities at the end of the traditional agriculture supply chain. Vertical indoor farming is a promising mode of next-generation agriculture that boasts reduced water and pesticide usage, improved yields, more consistent quality, year-round cultivation, and cheaper transportation and harvesting costs. Indoor farms can rival industrial greenhouses in size, but small-scale “pod farms" can be deployed to smaller communities and areas where large swaths of land are either unavailable or too costly. These pods are often the size of shipping containers with their temperature, humidity, and plant nutrient supply carefully controlled. Plants inside the pods are grown hydroponically with light supplied by panels of LEDs and, thus, this mode of farming is fundamentally different from greenhouse farming. Many indoor farming pods have recently become commercially available claiming high energy efficiency, but little analysis and optimization work has been done to prove these claims. To drive innovation in the design of these physical systems, we have developed a digital-twin and genomic optimization framework for the optical design of vertical indoor farming pods. We model a completely enclosed indoor farming pod with plants in the three mutually-orthogonal planes and illuminated by LED “walls." We employ ray-tracing methods and a genetic algorithm to determine the LED source tube area size, beam aperture spread, and power requirements for maximal power absorption by the plants.

Keywords Indoor farming · Optimization · Agriculture · Modeling and simulation · Machine-learning

1 Introduction

1.1 Vertical indoor farming

Indoor farming is a promising mode of next-generation agriculture, enabling year-round cultivation of produce, independent of local climate conditions. Indoor farms can be built in urban areas, making fresh, local produce available at lower prices to consumers, thanks to reduced transportation and irrigation costs. They also offer increased yields and reduced pesticide usage as, with soil-free hydroponics and a highly controlled growth environment, fewer plants are lost to pests and disease. In the face of a changing climate and “food deserts" prevalent in both urban and rural settings, indoor farming offers a sustainable solution to scarcity of fresh produce.

The concept of indoor farming has been explored for millennia. The concept of shielding plants from vacillating weather conditions by growing plants inside a greenhouse was first implemented by agrarian communities in 30 CE [1]. As time and technology progressed, full control over ventilation, air flow, growth medium, and light exposure became feasible. One of the first fully-fledged controlled environment research facilities began operation at North Carolina State University in 1968 [2]. Recent developments in the semiconductor industry have made it cost effective for light-emitting diodes (LEDs), which can provide the specific wavelengths of light for photosynthesis, to supplant broad-spectrum sunlight. This has given rise to “plant factories” [3] and indoor farming “pods” [4] (Fig. 1): warehouses and shipping containers outfitted with LEDs, hydroponics, cameras and advanced sensors which are nominally more efficient than traditional farms and greenhouses.

✉ Emre Mengi
emre_mengi@berkeley.edu

[1] Department of Mechanical Engineering, University of California, Berkeley, CA 94720-1740, USA

Published online: 05 December 2023

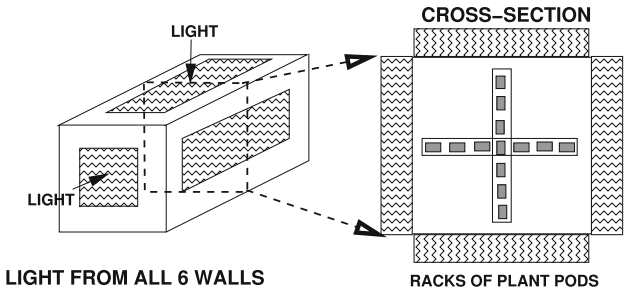

Fig. 1 A general schematic of an indoor container farming pod

Shade is not a concern for indoor farms as, with optimal optical design, all plants can receive the requisite light for photosynthesis. As such, many indoor farms will organize hydroponically grown plants in either 1) vertically-stacked shelves or 2) adjacent panels hanging from the ceiling [5]. This dense packing of plants facilitates more growth on less land. To put this into perspective, a 30-story vertical indoor farm with a 5-acre base could produce a crop yield equivalent to 2400 acres of a traditional farm [6].

1.2 LEDs: light-emitting diodes

Different plants require different wavelengths of light for optimal photosynthesis and optimal growth of features such as stem length and leaf thickness [7]. LEDs are perfectly suited to supply plants with the specific, optimal combination of colors of light they need, because LEDs emit a narrow band of wavelengths depending on the bandgap of their constituent semiconductor material. Thus, indoor pod farms with "walls" of LED light strips reduce energy waste by maximizing the amount of power absorbed by the plants and minimizing the power lost to excess heat. Beams of light supplied by LEDs can be collimated by addition of optical lenses, further reducing energy lost to non-plant targets and reducing the distance between the plants and LEDs. Additionally, exponential development in the semiconductor industry over the past three decades has made LEDs smaller, faster-actuating, more efficient, and more durable than traditional incandescent light sources, rendering LEDs economically viable for indoor farming applications.

1.3 Hydroponics

Hydroponics is a method of growing plants in a nutrient rich solution without the need for soil. Depending on the type of crop, this method can be executed via drip irrigation, aeroponics, nutrient film technique, ebb and flow, aquaponics, or deep-water culture. Although physically very different in the method of delivery, most of these techniques share the same fundamentals: a nutrient solution is pumped to the plants via a specialized delivery system and then circulated back to a reservoir where the nutrients are replenished. We refer the reader to [8–12] for a comprehensive description of these techniques. Hydroponic methods use, on average, 10% of the water utilized in traditional farming [13] as nutrients are delivered directly to the plant roots, minimizing water lost to evaporation. This mode of growing plants can be easily automated and, combined with the fact that the lack of soil protects against pests, these systems make it easier to cater to the unique physiological needs of the plants while eliminating the need for pesticides and other chemicals. These systems, however, have high start-up costs [14] and thus present a dire need for high operational efficiency to recoup these costs.

1.4 Digital-twins and optimization

The practice of vertical indoor farming in shipping container "pods," enabled by LED light sources and hydroponic nutrient sources, is still nascent and little work has been done to quickly and efficiently model and optimize such systems. A digital-twin of an indoor pod farm can be safely and cheaply manipulated without jeopardizing the system or the plants' well-being, making it an exceedingly quick, inexpensive, and useful approach for identifying optimal operational parameters.

The indoor farming pod is a complex system with a multitude of physical phenomena including air flow, light propagation, and energy transfer. Several digital-twin frameworks have been developed to capture the physics of light propagation in greenhouse, agrophotovoltaic, and food decontamination applications using ray tracing techniques [15–18] and to capture and optimize the physics of energy flow [19–21] and air flow [22, 23]. Ray tracing techniques decompose light into rays whose interactions with surfaces are quickly geometrically traced, facilitating fast computation of a large number of interactions between rays and surfaces and optimization of the surface shape for maximum absorption/reflection.

Digital-twins have been scarcely employed in optimizing agricultural systems [24–26], and they are even more rarely implemented in indoor farming pods. Two such implementations were carried out by Randolph et al. [27] and Sambor et al. [28] to optimize the energy consumption of an off-grid indoor farming pod to determine optimal operation time for each component of the system. These implementations, however, do not allow for manipulation of the orientation and/or shape of the system's components for maximum operational efficiency. In [29], computational fluid dynamics (CFD) methods were utilized to model the air flow inside an indoor farming pod, but such methods have a prohibitively high computational cost, especially when running various configurations and performing optimization. Thus, an easily

manipulated, computationally inexpensive model that accurately captures the system's physics is desired.

1.5 Objectives

Over the past few years, around the world, many indoor farming companies have been proving that indoor farming is a viable mode of next-generation farming, but the systems remain energy-intensive and little analysis has been performed to assess system efficiency. To optimize these systems and drive innovative solutions, this work develops a flexible digital-twin for the optical design of sustainable, small-scale indoor farming "pods," containing vertically grown plants with energy supplied by carefully controlled LEDs. Flow of LED power is rapidly computed with a reduced order model of Maxwell's equations based on high-frequency decomposition of the LED irradiance into multiple rays. These rays are then propagated forward in time to track their reflections and ultimate absorption. We simulate thousands of source-system configurations, varying the emission characteristics of the LED "walls" and optimizing for maximal power absorption by the plant "targets."

Our digital-twin consists of

- A model for the LED optics and tracking of power flow,
- A model for the absorption of the optical power by the pod components, and
- A genomic optimization of LED configuration and emission characteristics.

Our digital-twin and optimization framework described in this work can be quickly and easily run on a laptop, making it more accessible than computationally-intensive alternatives. This work is motivated by the possibility that indoor farming researchers and practitioners will tailor this simulation paradigm for their specific system's needs.

2 Indoor farming model

2.1 Pod farm, plant, and LED geometries

We model an indoor pod farm as an enclosed rectangular box defined by "wall cutoff" values $(x_{w1\pm}, x_{w2\pm}, x_{w3\pm})$ which can be adjusted to simulate any pod size. Each wall has an array of LEDs whose beam spread, power, and geometric configuration (limited to a rectangle within the wall plane) can be configured for optimal performance. We can label the six walls by their inward surface normal in the standard Euclidean basis $(\boldsymbol{e}_1, \boldsymbol{e}_2, \boldsymbol{e}_3)$. Using Cartesian coordinates (x_1, x_2, x_3), we designate the center of the pod as the origin. Plants racks can then exist in planes parallel to $x_1 = 0$, $x_2 = 0$, and/or $x_3 = 0$. Example plant rack configurations are shown in Fig. 2.

Once rays are emitted from one of the six walls of the pod, they are propagated forward in time. In each time step, we check to see if the ray has hit a wall or a plant or will simply continue propagating as in the previous time step. Once a ray-surface interaction happens, we determine the power absorbed by either the wall or plant, the residual power in the ray, and reflection normal for the ray.

Plant targets are modeled as generalized ellipsoids. We define the surface of plant i with

$$\begin{aligned} F_i(x_1, x_2, x_3) &= \left|\frac{x_1 - x_{1i}}{R_1}\right|^{q_1} + \left|\frac{x_2 - x_{2i}}{R_2}\right|^{q_2} + \left|\frac{x_3 - x_{3i}}{R_3}\right|^{q_3} \\ &\leq 1 \end{aligned} \tag{2.1}$$

where (R_1, R_2, R_3) are the generalized radii, (q_1, q_2, q_3) are the generalized exponents, and (x_{1i}, x_{2i}, x_{3i}) define the center of the plant.

For ray j at location (x_{1j}, x_{2j}, x_{3j}), if

$$\begin{cases} x_{1j} \leq x_{w1-} & \text{or} \\ x_{1j} \geq x_{w1+} & \text{or} \\ x_{2j} \leq x_{w2-} & \text{or} \\ x_{2j} \geq x_{w2+} & \text{or} \\ x_{3j} \leq x_{w3-} & \text{or} \\ x_{3j} \geq x_{w3+}, \end{cases} \tag{2.2}$$

then we say the ray has hit a wall. If for plant target i

$$F_i(x_{1j}, x_{2j}, x_{3j}) \leq 1, \tag{2.3}$$

then we say that ray j has hit plant i.

2.2 Initializing rays

Ray positions, $\boldsymbol{r}(x_1, x_2, x_3)$, are randomly initialized within a rectangular area defined by the "source tube" values ST_{1-12} (defined in Table 1) on the surface one of the six walls. For example, for the wall with surface normal $+\boldsymbol{e}_1$, rays will emanate from the point

$$\begin{cases} x_1 = x_{w1+}, \\ x_2 \in_{\text{rand}} [-ST_{11}, ST_{11}], \\ x_3 \in_{\text{rand}} [-ST_{12}, ST_{12}]. \end{cases} \tag{2.4}$$

As there are six walls and two source tube values per wall, there are a total of 12 source tube values.

Ray velocities, $\boldsymbol{v}$, are initialized with magnitudes equal to the speed of light and directions randomly determined from a set of "aperture" values A_{1-18}. As there are six walls and three aperture values per wall, there are a total of 18 aperture values. Once a direction of travel is determined from the

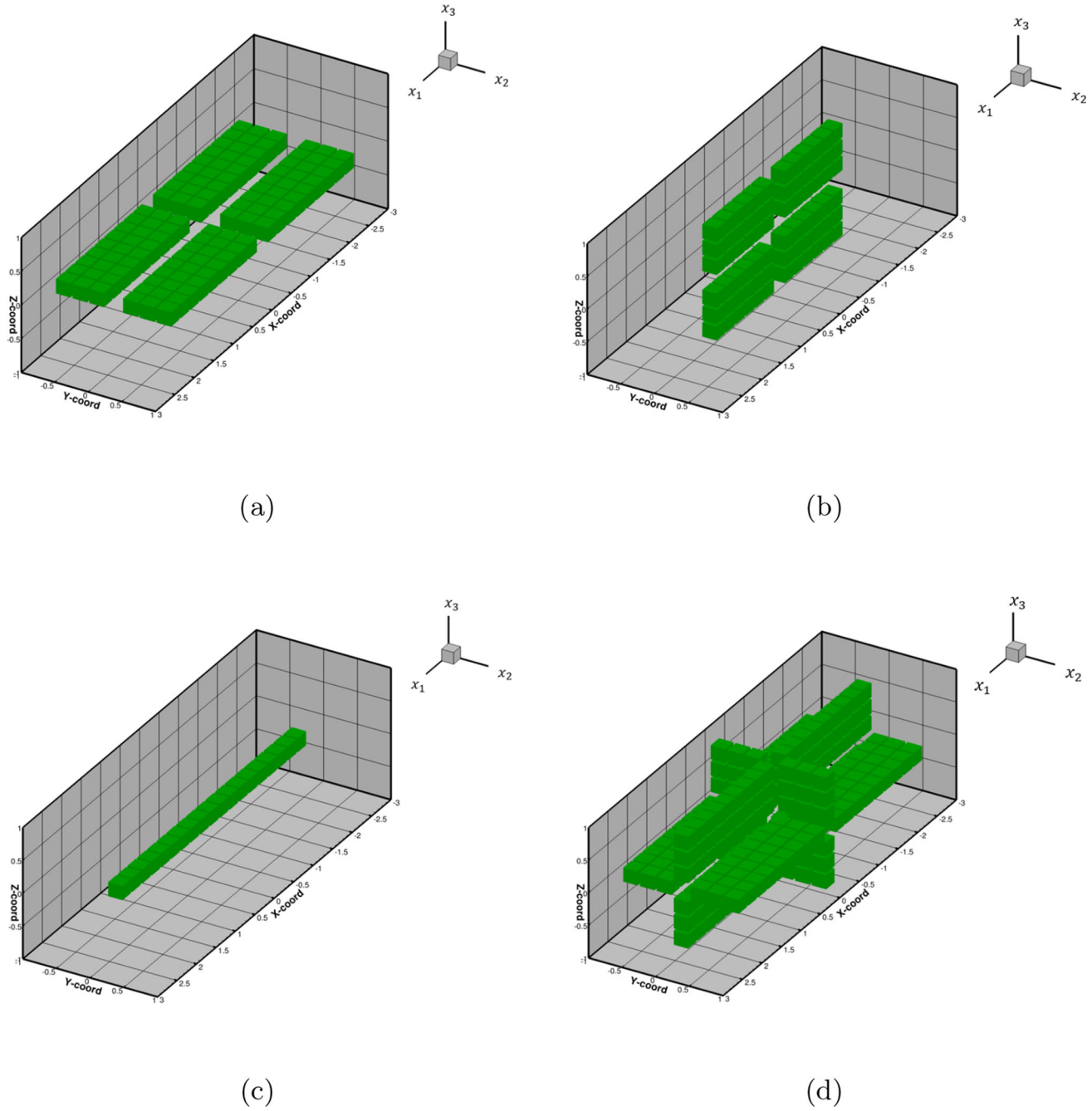

Fig. 2 Example pod configurations for **a** rack: x_1x_2, number of targets: $x_1 : 9$, $x_2 : 3$, **b** rack: x_1x_3, number of targets: $x_1 : 6$, $x_3 : 3$, **c** rack: x_1, number of targets: $x_1 : 9$, and **d** racks: x_1x_2, x_1x_3, x_2x_3, number of targets: $x_1 : 9$, $x_2 : 3$, $x_3 : 3$. Plants are visualized as cubes for plot simplicity

Table 1 Design parameters associated with each wall

Inward normal	Aperture parameters	Source tube parameters [m]	Power parameters [W]
$-\boldsymbol{e}_1$	A_1, A_2, A_3	ST_9, ST_{10}	P_1
$\boldsymbol{e}_1$	A_4, A_5, A_6	ST_{11}, ST_{12}	P_2
$-\boldsymbol{e}_2$	A_7, A_8, A_9	ST_5, ST_6	P_3
$\boldsymbol{e}_2$	A_{10}, A_{11}, A_{12}	ST_7, ST_8	P_4
$-\boldsymbol{e}_3$	A_{13}, A_{14}, A_{15}	ST_3, ST_4	P_5
$\boldsymbol{e}_3$	A_{16}, A_{17}, A_{18}	ST_1, ST_2	P_6

aperture values, the direction is normalized and then scaled by the speed of light. That is, we first determine the unnormalized components of the direction (a_1, a_2, a_3):

$$\begin{cases} a_1 \in_{\text{rand}} [0, A_{x_1}], \\ a_2 \in_{\text{rand}} [0, A_{x_2}], \\ a_3 \in_{\text{rand}} [0, A_{x_3}], \end{cases} \tag{2.5}$$

then normalize

$$\begin{cases} \hat{v}_1 = \dfrac{a_1}{||\boldsymbol{a}||}, \\ \hat{v}_2 = \dfrac{a_2}{||\boldsymbol{a}||}, \\ \hat{v}_3 = \dfrac{a_3}{||\boldsymbol{a}||}, \end{cases} \tag{2.6}$$

where $||\boldsymbol{a}|| = \sqrt{a_1 + a_2 + a_3}$. Finally, we scale by the speed of the light, c, to obtain the components of the full initial velocity vector:

$$\begin{cases} v_1 = c\hat{v}_1, \\ v_2 = c\hat{v}_2, \\ v_3 = c\hat{v}_3. \end{cases} \tag{2.7}$$

Initial ray position and velocity determination is visualized in Fig. 3.

Ray power values are initialized as a fraction of the total power, P_w, coming from the wall associated with the initial ray position. If the total number of rays coming from the wall is N_r, then the power in each ray emanating from wall w is

$$P_{\text{ray}} = \frac{P_w}{N_r}. \tag{2.8}$$

As there are six walls and one total power value per wall, there are a total of 6 wall power parameters P_{1-6}. The source tube, aperture, and wall power parameters comprise the 36 design parameters for optimization in this study.

2.3 Ray-tracing method

We followed a similar approach to that in Isied et al. [18] for computing the trajectories of the reflected and the absorbed rays. We assume the rays travel in a vacuum at the speed of light ($c \approx 3 \times 10^8\ m/s$) with refractive index $n_i = 1$. While individually adjustable, for ease of description, we say the indices of refraction of each wall and of the plants are all n_a. For later use determining how much power will be reflected/absorbed by either the plants or the pod walls, we define the ratio

$$\hat{n} = \frac{n_a}{n_i}. \tag{2.9}$$

In the process of propagating all of the rays in the simulation, if we determine that a ray has hit a plant surface, we first calculate the reflection normal for the ray. If the surface of the plant i is defined by $F_i(x_1, x_2, x_3)$, given in (2.1), then the surface normal is given by

$$\boldsymbol{n} = \frac{\nabla F_i}{||\nabla F||} \tag{2.10}$$

where, in terms of a standard Euclidean basis $(\boldsymbol{e}_1, \boldsymbol{e}_2, \boldsymbol{e}_3)$,

$$\nabla F_i = \frac{\partial F}{\partial x_1}\boldsymbol{e}_1 + \frac{\partial F}{\partial x_2}\boldsymbol{e}_2 + \frac{\partial F}{\partial x_3}\boldsymbol{e}_3, \tag{2.11}$$

or more completely, by calculating the gradient of Eq. 2.1,

$$\nabla F_i = \begin{pmatrix} \dfrac{x_1}{|x_1|}\dfrac{q_1}{R_1}\left(\dfrac{x_1 - x_{1i}}{R_1}\right)^{q_1-1} \\ \dfrac{x_2}{|x_2|}\dfrac{q_2}{R_2}\left(\dfrac{x_2 - x_{2i}}{R_2}\right)^{q_2-1} \\ \dfrac{x_3}{|x_3|}\dfrac{q_3}{R_3}\left(\dfrac{x_3 - x_{3i}}{R_3}\right)^{q_3-1} \end{pmatrix}. \tag{2.12}$$

If the ray hits the surface at angle θ_{inc} with respect to the surface normal, then the reflected velocity $\boldsymbol{v}_{\text{ref}}$ is given by

$$\boldsymbol{v}_{\text{ref}} = \boldsymbol{v}_{\text{inc}} - 2\boldsymbol{v}_{\text{inc},\perp} \tag{2.13}$$

where $\boldsymbol{v}_{\text{inc},\perp}$ is the component of the incident velocity $\boldsymbol{v}_{\text{inc}}$ perpendicular to the surface (and parallel to the surface normal), given by

$$\boldsymbol{v}_{\text{inc},\perp} = \boldsymbol{v}_{\text{inc}} \cdot \boldsymbol{n} = ||\boldsymbol{v}_{\text{inc}}|| \cos\theta_{\text{inc}}. \tag{2.14}$$

If we determine that a ray has hit a wall, we simply flip the sign of the component of the velocity parallel to the wall surface normal e.g. if a ray hits the wall with inward surface normal $+\boldsymbol{e}_1$, then

$$\begin{cases} v_{\text{ref},1} = -v_{\text{inc},1} \\ v_{\text{ref},2} = \ \ v_{\text{inc},2} \\ v_{\text{ref},3} = \ \ v_{\text{inc},3} \end{cases}. \tag{2.15}$$

After calculating the reflection normal for the ray, we must calculate the power absorbed by the contact surface and the residual power left in the ray. Following Zohdi [17], we define the ratio of the reflected power of the ray, I_{ref}, to the incident power, I_{inc}, as the total reflectance, $\mathcal{R}$:

$$\mathcal{R} = \frac{I_{\text{ref}}}{I_{\text{inc}}}. \tag{2.16}$$

The total reflectance is a function of the angle of incidence and the ratio of the refractive indices $\hat{n}$, given in (2.9). We

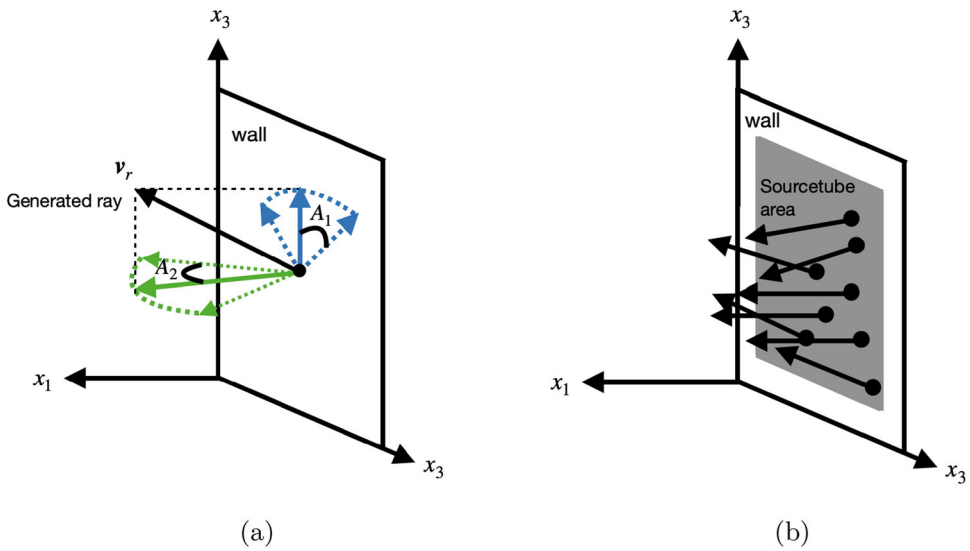

Fig. 3 **a** Aperture settings determining initial ray direction **b** Source tube parameters determining ray initialization area

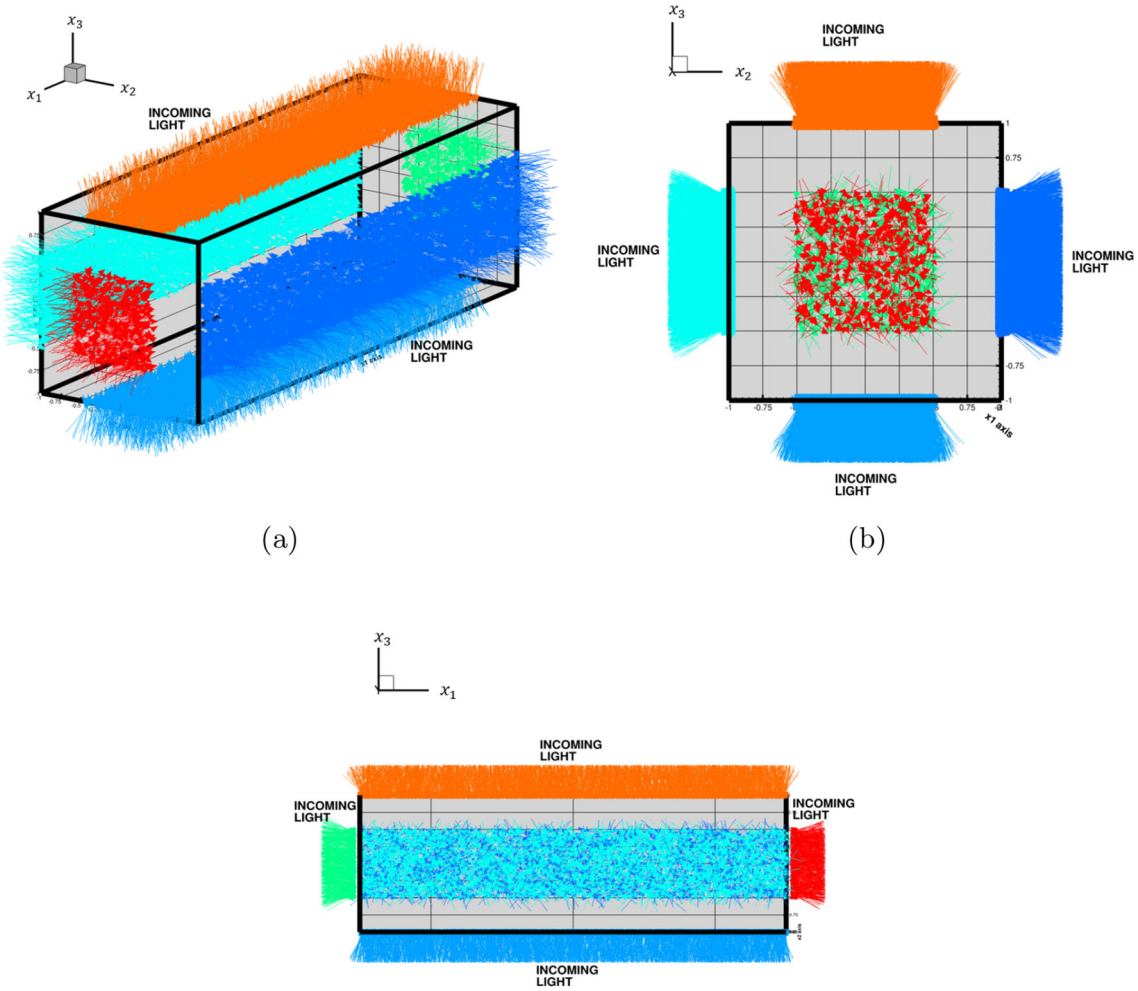

Fig. 4 Ray initialization with 6 walls, aperture values A_{1-18} : 0.5 and source tube lengths ST_{1-4} : 0.5 and ST_{5-12} : 3. Ray color added for visual clarity

refer the reader to Zohdi [17] for the details of the derivation. The expanded form of the reflectance is

$$\mathcal{IR}(\hat{n},\theta) = \frac{1}{2}\left(\frac{\hat{n}^2\cos\theta - (\hat{n}^2-\sin^2\theta)^{1/2}}{\hat{n}^2\cos\theta + (\hat{n}^2-\sin^2\theta)^{1/2}}\right)^2 + \frac{1}{2}\left(\frac{\cos\theta - (\hat{n}^2-\sin^2\theta)^{1/2}}{\cos\theta + (\hat{n}^2-\sin^2\theta)^{1/2}}\right)^2 \tag{2.17}$$

where $0 \leq \mathcal{IR} \leq 1$ for unpolarized electromagnetic radiation and we have set $\theta = \theta_{\text{inc}}$ and implicitly assumed that the magnetic permeability of the plants, walls, and ambient medium are all equal.

The power absorbed by the surface, P_{abs}, and the power retained by the ray, P_{ref}, are computed as:

$$\begin{cases} P_{\text{abs}} = (1-\mathcal{IR})P_{\text{inc}} \\ P_{\text{ref}} = \mathcal{IR}P_{\text{inc}} \end{cases} \tag{2.18}$$

where P_{inc} is the incident power. Ray power values are updated in each time step until the power in the ray falls below some threshold. At that point, the ray is considered fully absorbed and deactivated.

2.4 Time-stepping scheme

The power propagation scheme outlined in the previous section is achieved through an explicit time-stepping scheme with a time step size defined by

$$\Delta t = \left(\frac{\Delta x_1 + \Delta x_2 + \Delta x_3}{3c}\right)\xi \tag{2.19}$$

where $(\Delta x_1, \Delta x_2, \Delta x_3)$ are the voxel sizes per axis, c is the speed of light, and ξ is a tunable parameter for refining the step size. Voxel sizes and ξ are constants defined at the start of the simulation. With higher values of ξ, the simulation runs faster and with lower values of ξ the collisions are modeled more accurately. In this study, we use $\xi = 2$ to accurately capture the ray interactions without significantly slowing down the simulation. A convergence study could be conducted by including ξ in the set of design parameters for more refinement, but this is beyond the scope of this study.

The time-stepping algorithm for all rays $j = 1, \ldots, N_r$ starting at time $t = 0$ and terminating at $t = T$ can be summarized as follows:

1. Initialize ray velocities $\boldsymbol{v}_j(t=0)$ and positions $\boldsymbol{r}_j(t=0)$.
2. Increment all ray positions:

$$\boldsymbol{r}_j(t+\Delta t) = \boldsymbol{r}_j(t) + \Delta t\boldsymbol{v}_j(t). \tag{2.20}$$

3. Check for ray-surface collisions. If a ray has collided with a surface:
   (a) Calculate the surface normal,
   (b) Calculate the new ray velocity values after reflection,
   (c) Update power absorbed by the surface if it is a plant,
   (d) Update the new ray power after reflection.
4. Increment the time forward by Δt. If $t < T$, then go to step 2.

3 Machine-learning, optimization, and automatic design

3.1 Design parameters

The indoor farming system design consists of the following 36 design parameters:

$$\begin{aligned} \Lambda^i &\equiv \{\Lambda^i_1, \ldots, \Lambda^i_N\} \\ &\equiv \{A_1, \ldots, A_{18}, ST_1, \ldots, ST_{12}, P_1, \ldots, P_6\} \end{aligned} \tag{3.1}$$

where A_{1-18} are the aperture parameters (3 per wall) are used to determine the initial light direction, ST_{1-12} are the source tube values (2 per wall) that dictate the wall area in which the ray will be randomly initialized, and P_{1-6} are the total power values (1 per wall). Table 1 outlines which design parameters belong to each wall, where each wall is identified by its inward normal in the standard Euclidean basis.

3.2 Design fitness

The 36 design parameters define a design space which we can explore and evaluate with a cost function. Different parameter sets will result in different indoor farming system performance with lower values of the cost function corresponding to stronger design fitness. The definition of design fitness may differ between applications and the cost function can be tailored to each application. In this study, we seek to maximize the power absorbed by the plants inside the indoor farming pod. Accordingly, we construct the cost function

$$\Pi = 1 - \frac{\sum_{i=1}^{N_p} P_i}{\sum_{w=1}^{6} P_w} \tag{3.2}$$

where N_p is the total number of plants and the sum over P_w values represents the total initial power emitted by all 6 walls. Our genomic optimization scheme will attempt to minimize Π, which ultimately maximizes the power absorbed by the targets. Note that the ratio of power absorbed over power irradiated in the cost function is non-dimensional and normalized.

3.3 Machine-learning optimization scheme: genetic algorithm

The indoor farming digital-twin presented in this work was optimized using a genetic algorithm (GA) to find the design parameter set that minimizes the cost function in (3.2). A genetic algorithm is a sampling-based optimization scheme for solving black-box objectives. Genetic algorithms are inspired by the process of natural selection wherein the fittest members of a population survive to breed offspring, potentially with even stronger characteristics. The genetic algorithm parameters and design parameter search bounds used in this work are included in Table 3. The genetic algorithm framework is shown in Fig. 6 and can be summarized as follows:

1. Generate `S` genetic strings, where the design parameters comprising each string are randomly selected from a range defined by search bounds. That is, produce a population

$$\mathbf{\Lambda} = \{\mathbf{\Lambda}^{(1)}, \mathbf{\Lambda}^{(2)}, \ldots, \mathbf{\Lambda}^{(S)}\} \tag{3.3}$$

where

$$\mathbf{\Lambda}^{(i)} = \begin{pmatrix} A_1^- \le A_1^{(i)} \le A_1^+ \\ \vdots \\ A_{18}^- \le A_{18}^{(i)} \le A_{18}^+ \\ ST_1^- \le ST_1^{(i)} \le ST_1^+ \\ \vdots \\ ST_{12}^- \le ST_{12}^{(i)} \le ST_{12}^+ \\ P_1^- \le P_1^{(i)} \le P_1^+ \\ \vdots \\ P_6^- \le P_6^{(i)} \le P_6^+ \end{pmatrix} \quad \text{for} \quad i = 1, \ldots, \mathtt{S}. \tag{3.4}$$

2. Compute the fitness of each string by evaluating the cost function from the proposed indoor farming configuration i.e. $\Pi(\mathbf{\Lambda}^{(i)})$ for $i = 1, \ldots, \mathtt{S}$.
3. Rank the genetic strings such that the best string has the lowest cost.
4. Pairwise mate the top `P` genetic strings with randomized weights ϕ_1 and ϕ_2 to obtain `K` offspring i.e. parents p and $p+1$ will produce offspring k and $k+1$ according to

$$\begin{cases} \mathbf{\Lambda}^{(k)} &= \phi_1 \mathbf{\Lambda}^{(p)} + (1-\phi_1)\mathbf{\Lambda}^{(p+1)} \\ \mathbf{\Lambda}^{(k+1)} &= \phi_2 \mathbf{\Lambda}^{(p)} + (1-\phi_2)\mathbf{\Lambda}^{(p+1)} \end{cases} \tag{3.5}$$

where $\phi_1, \phi_2 \in_{\text{rand}} [0, 1]$.
5. Retain the top performing `P` parent strings and their `K` children and generate `S-P-K` new random genetic strings, maintaining the size of the population.

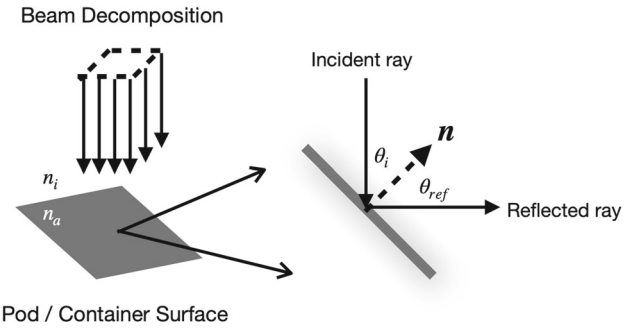

Fig. 5 Beam decomposition for a geometric ray-tracing model

6. Every 10 generations, allow the population to "re-adapt" by updating the search bounds to be a range about the values of the best string thus far.
7. Repeat steps 2-6 with until `G` generations have been reached.

4 Results and discussion

We simulated a completely enclosed indoor farm with LED light sources on all six walls using the previously described digital-twin framework and optimization scheme. The dimensions of the simulated farming pod were $6 \times 1 \times 1$ m. We allowed racks of plants to exist in the x_1x_2, x_1x_3 and x_2x_3 planes with generalized radii $R_1 = R_2 = R_3 = 0.1375$ m and generalized exponents $q_1 = q_2 = q_3 = 6$, effectively simulating the plants as bevelled cubes with volume $0.1375\,\text{m}^3$. For the racks in planes x_1x_2 and x_1x_3 there were $18 \times 6 = 108$ plants each and for the rack in plane x_2x_3 there were $6 \times 6 = 36$ plants, meaning the pod farm contained 252 plants in total. In each time step, we tracked the power absorbed by each plant, the fraction of rays interacting with a plant, and the total number of ray-surface interactions. Figure 8 shows the relative power absorption of different plants with red corresponding to the highest power absorption and blue corresponding to the lowest power absorption. While adjustable, we set the indices of refraction for the 6 walls to ($n_{w1-} = 10.0, n_{w1+} = 4.0, n_{w2-} = 1.5, n_{w2+} = 3.0, n_{w3-} = 9.0, n_{w3+} = 2.0$) and the index of refraction of the ambient container medium to $n_i = 1$. In all simulation figures in this work, a unique ray color denotes a distinct wavelength, but wavelength was not accounted for by the ray-tracing method used. Each wall $w = 1, \ldots, 6$ was initialized with power $P_w \in_{\text{rand}} 1 - 10$ MW and with ray density 2000 rays per source tube area. The indoor farming system parameters and the genetic algorithm parameters for optimization used in this study are included in Tables 2 and 3 respectively.

When simulating with equal index of refraction among all walls and plants, we found that the best design reduced

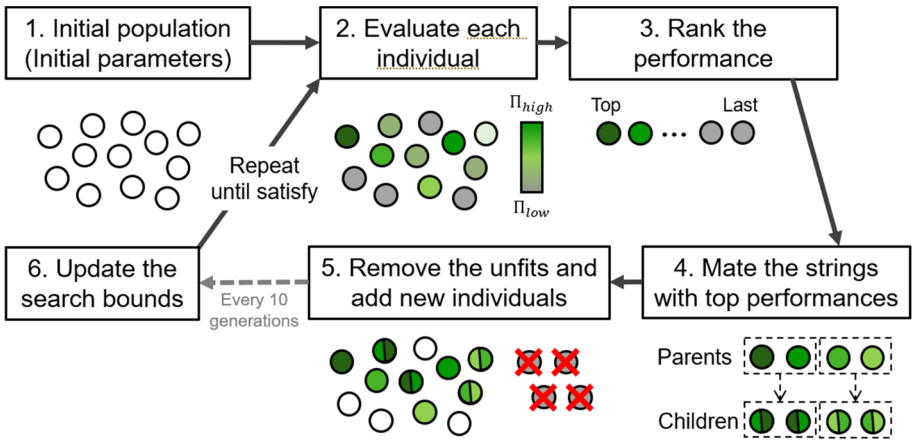

Fig. 6 The genetic algorithm framework used in this study

Table 2 Indoor farming system parameters

Symbol	Units	Value	Description
N_r	none	2000	Number of rays per wall
`activeRacks`	none	x_1x_3, x_1x_2, x_2x_3	Active rack axes/planes
$N_{p,\pm1}, N_{p,\pm2}, N_{p,\pm3}$	none	[9, 3, 3]	Number of plants per axis
$\Delta x_1, \Delta x_2, \Delta x_3$	none	0.05	Voxel size
c	m/s	3×10^8	Speed of light
R_1, R_2, R_3	m	$2.75\Delta x$	Generalized radii
q_1, q_2, q_3	none	6	Generalized exponents

Table 3 Genetic algorithm parameters

Symbol	Units	Value	Description
`P`	none	4	Surviving parent strings for breeding
`K`	none	4	Number of offspring per generation
`S`	none	24	Designs per generation
`G`	none	150	Total generations
A_{1-18}	none	[0, 1]	Aperture parameters
ST_{1-4}	m	[0, 0.5]	Source tube search bounds
ST_{5-12}	m	[0, 3]	Source tube search bounds
P_{1-6}	MW	[1, 10]	Total wall power search bounds

the source tube areas to more closely overlap with the plant racks, increasing the ray density per source tube area and increasing the number of rays directly incident on the plants. With a larger number of rays directly incident on the plants, the number of reflections a ray makes is reduced, thereby decreasing the energy waste from reflections with each surface.

Optimal results are visualized in Figs. 7 and 8 and were produced using the design parameters in Table 4. Comparing Fig. 4 (no optimization) with Fig. 7, we can see that the optimization algorithm favors a smaller source tube area on all six walls to maximize overlap with the plant rack locations. The relatively small optimal source tube areas depicted in Fig. 8 can be attributed to not specifying a power absorption limit for the closest plant targets. The evolution of the best design cost and average design cost across the population over 150 generations with 24 design strings per population is included in Fig. 9. Every 10 generations, we allowed the population to re-adapt by redefining the search bounds for each design parameter to be a range about the parameter values of the best string seen thus far.

These results serve to demonstrate a framework for the modeling and optimization of an indoor farming pod. This framework can be modified to better capture all aspects of the system by extending the design parameters and modeling other physical phenomena such as water absorption, air flow, multi-wavelength energy tracking, and setting power absorption caps for different plant types.

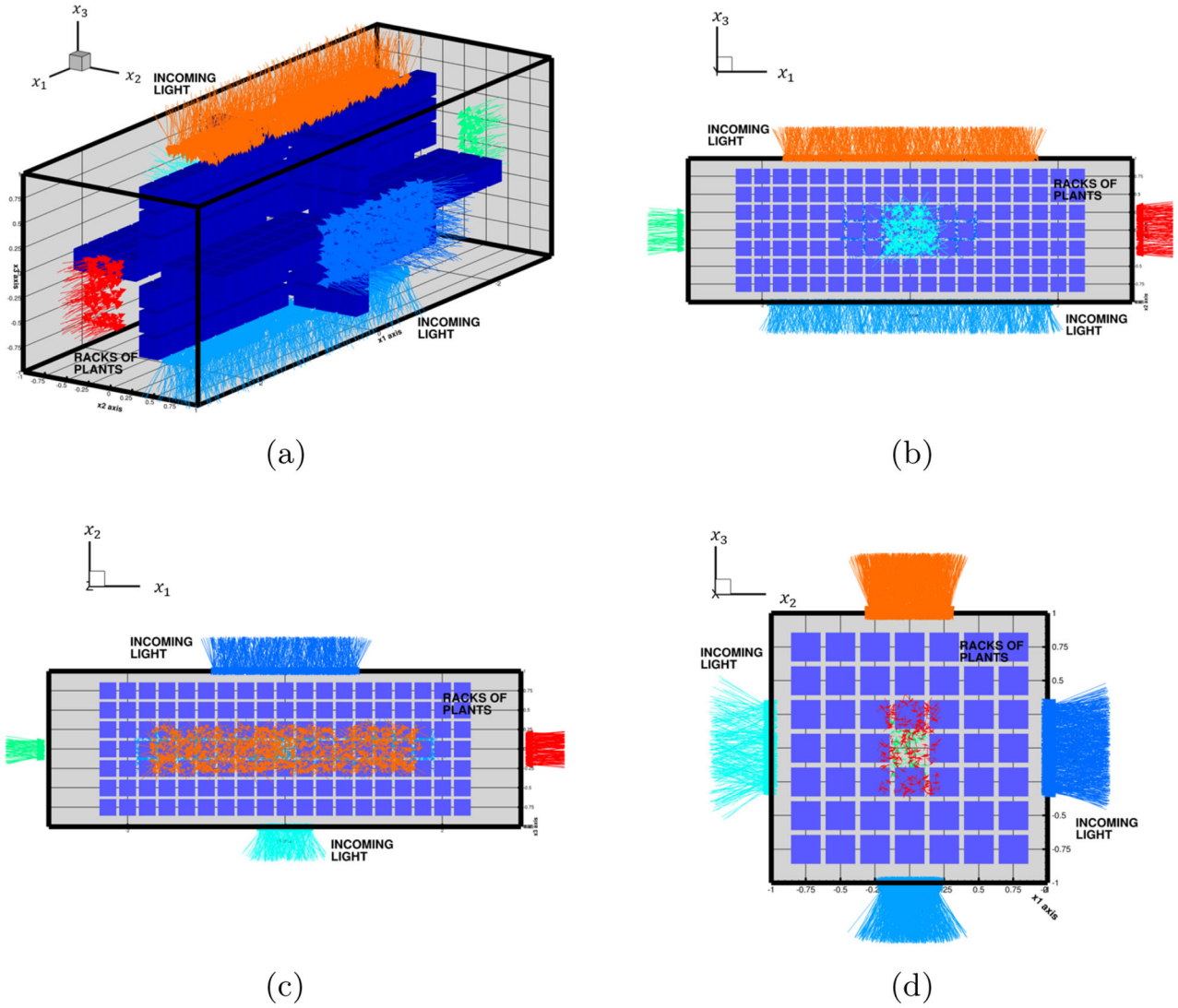

Fig. 7 Detailed views of optimized indoor farming system design. Ray color added for visual clarity. **a** Isometric view of optimized indoor farming design. **b** Side view of optimized indoor farming design. **c** Top view of optimized indoor farming design. **d** Front view of optimized indoor farming design.

5 Summary and model extensions

Indoor farming is a promising mode of next-generation agriculture offering numerous benefits such as year-round crop cultivation, reduced transportation costs, and enablement of urban farms. However, these systems still face challenges related to energy consumption, and there has been limited quantitative analysis of their overall efficiency. To fill this gap and promote innovative design, we introduce a cost-effective digital-twin to analyze the optical properties of an indoor farming pod using a ray-tracing model. We utilize a genomic optimization scheme to identify the most optimal LED geometric configurations and emission characteristics toward maximizing energy absorbed by the constituent plants. The proposed digital-twin and optimization framework serves as a foundational framework that takes a physics-driven approach to optimize energy flow and paves the way for more sustainable indoor farming practices.

To adapt the framework to other indoor farming configurations, we can adjust design objectives via cost function design and incorporate constraints via parameter search bounds. The framework could also be extended to include models for water usage or crop-specific reactions to different chemical/pesticides, thereby enhancing the accuracy of the digital-twin. Extending the framework to include wavelength-specific power flow could further improve predictions of energy efficiency and crop yield by providing each plant with its ideal lighting conditions. Such refined models can serve as a valuable tools for testing and estimating how a particular design would perform in the real world, enabling

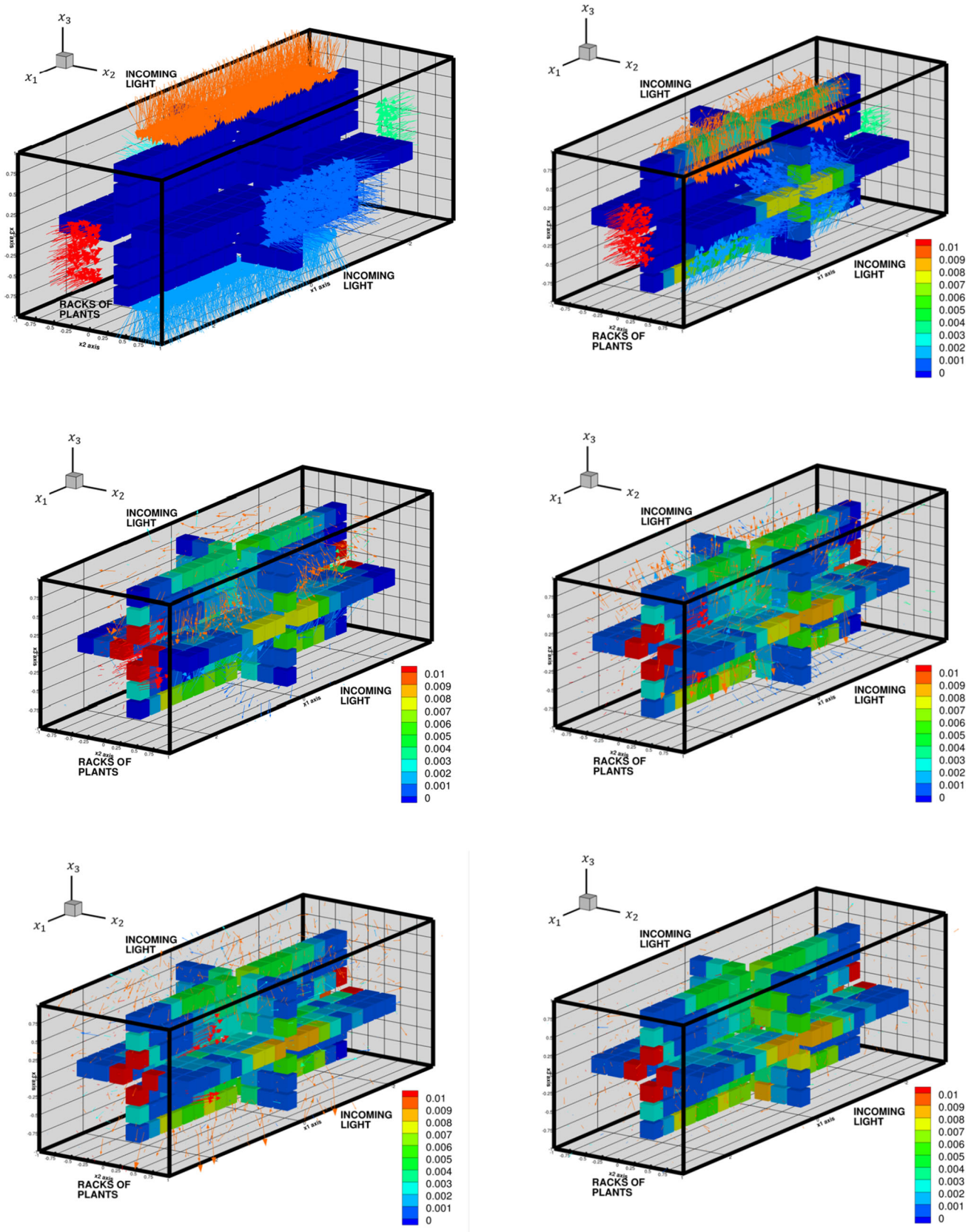

Fig. 8 Optimal indoor farming system light pulse snapshots. Ray color added for visual clarity. Colorbar added to show differential power absorption by plants. Red corresponds to higher power absorption and blue to lower power absorption

Table 4 Optimal indoor farming design parameters corresponding to $\Pi_{\text{best}} = 0.153$. aperture values are unitless. Source tube values in meters. Power values in megawatts

A_1	A_2	A_3	A_4	A_5	A_6
0.567	0.108	0.174	0.636	0.216	0.195
A_7	A_8	A_9	A_{10}	A_{11}	A_{12}
0.515	0.252	0.421	0.740	0.416	0.578
A_{13}	A_{14}	A_{15}	A_{16}	A_{17}	A_{18}
0.586	0.394	0.198	0.597	0.690	0.199
ST_1	ST_2	ST_3	ST_4	ST_5	ST_6
1.909	0.207	1.692	0.295	0.326	0.328
ST_7	ST_8	ST_9	ST_{10}	ST_{11}	ST_{12}
0.914	0.334	0.120	0.283	0.215	0.360
P_1	P_2	P_3	P_4	P_5	P_6
5.66	5.68	7.22	6.29	3.28	4.03

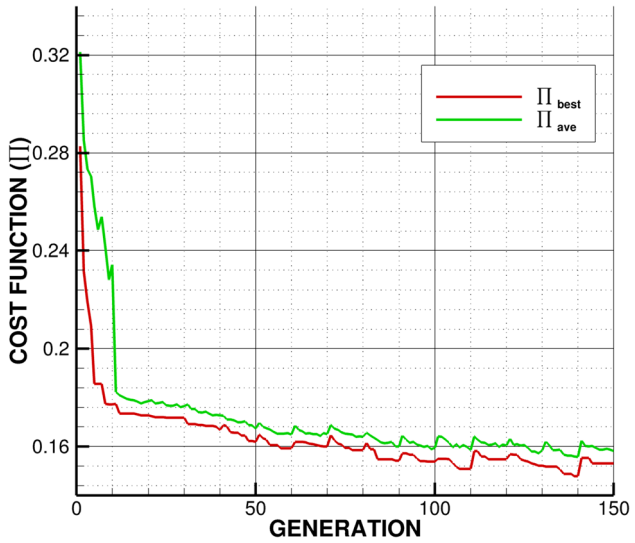

Fig. 9 Cost function evolution over 150 generations. The plot shows the cost of the best performing design (*red*) and the average cost of the entire population (*green*) as a function of successive generations. The GA was allowed to re-adapt every 10 generations. The lowest cost in generation 1 was $\Pi_{\text{best}}^{g=1} \approx 0.2826$ and was reduced to $\Pi_{\text{best}}^{g=150} \approx 0.1531$ by generation 150. This is a reduction of $\sim 45.82\%$

farmers to make informed decisions and effectively optimize their own indoor farming setups.

Acknowledgements This work has been partially supported by the UC Berkeley College of Engineering and the USDA AI Institute for Next Generation Food Systems (AIFS), USDA award number 2020-67021-32855.

Declaration

Conflict of interest The authors declare that they have no known competing financial interests or personal relationships that could have appeared to influence the work reported in this paper.

References

1. Mitchell CA (2022) History of controlled environment horticulture: indoor farming and its key technologies. HortScience 57:247–256. https://doi.org/10.21273/HORTSCI16159-21
2. Kramer PJ, Hellmers H, Downs RJ (1970) Sepel: new phytotrons for environmental research. BioScience 20:1201–1208. https://doi.org/10.2307/1295626
3. Kozai T (2018) Smart plant factory. Springer Singapore. https://doi.org/10.1007/978-981-13-1065-2
4. Freight farms. https://www.freightfarms.com/home/
5. Beacham AM, Vickers LH, Monaghan JM (2019) Vertical farming: a summary of approaches to growing skywards. J Hortic Sci Biotechnol 94:277–283. https://doi.org/10.1080/14620316.2019.1574214
6. Al-Kodmany K (2 2018) The vertical farm: a review of developments and implications for the vertical city. Buildings, 8 . https://doi.org/10.3390/buildings8020024
7. Massa GD, Kim H-H, Wheeler RM, Mitchell CA (2008) Plant productivity in response to led lighting. HortScience 43:1951–1956. https://doi.org/10.21273/HORTSCI.43.7.1951
8. Khan S, Purohit A, Vadsaria N (2020) Hydroponics: current and future state of the art in farming. J Plant Nutr 44:1515–1538. https://doi.org/10.1080/01904167.2020.1860217
9. Velazquez-Gonzalez R S, Garcia-Garcia A L, Ventura-Zapata E, Barceinas-Sanchez J D O, Sosa-Savedra J C (5 2022) A review on hydroponics and the technologies associated for medium-and small-scale operations. Agriculture (Switzerland), 12. https://doi.org/10.3390/agriculture12050646
10. Fussy A, Papenbrock J (5 2022) An overview of soil and soilless cultivation techniques-chances, challenges and the neglected question of sustainability. Plants, 11. https://doi.org/10.3390/plants11091153
11. Eldridge BM, Manzoni LR, Graham CA, Rodgers B, Farmer JR, Dodd AN (2020) Getting to the roots of aeroponic indoor farming. New Phytol 228:1183–1192. https://doi.org/10.1111/nph.16780
12. Niu G, Masabni J (2022) Hydroponics. Elsevier. https://doi.org/10.1016/B978-0-323-85152-7.00023-9
13. Sharma N, Acharya S, Kumar K, Singh N, Chaurasia O (2018) Hydroponics as an advanced technique for vegetable production: an overview. J Soil Water Conserv 17:364. https://doi.org/10.5958/2455-7145.2018.00056.5
14. Souza SV, Gimenes RMT, Binotto E (2019) Economic viability for deploying hydroponic system in emerging countries: a differentiated risk adjustment proposal. Land Use Policy 83:357–369. https://doi.org/10.1016/j.landusepol.2019.02.020
15. Zohdi T (2020) Rapid simulation of viral decontamination efficacy with uv irradiation. Comput Methods Appl Mecha Eng 369:113216. https://doi.org/10.1016/j.cma.2020.113216
16. Mengi E, Samara OA, Zohdi TI (2023) Crop-driven optimization of agrivoltaics using a digital-replica framework. Smart Agric Technol 4:100168. https://doi.org/10.1016/j.atech.2022.100168
17. Zohdi TI (2021) A digital-twin and machine-learning framework for the design of multiobjective agrophotovoltaic solar farms. Comput Mech 68:357–370. https://doi.org/10.1007/s00466-021-02035-z
18. Isied R S, Mengi E, Zohdi T I (11 2022) A digital-twin framework for genomic-based optimization of an agrophotovoltaic greenhouse system. In: Proceedings of the royal society a: mathematical, physical and engineering sciences, 478. https://doi.org/10.1098/rspa.2022.0414
19. Zohdi T (2023) A machine-learning digital-twin for rapid large-scale solar-thermal energy system design. Comput Methods Appl Mech Eng 412:115991. https://doi.org/10.1016/j.cma.2023.115991

20. Zohdi TI (2022) An adaptive digital framework for energy management of complex multi-device systems. Comput Mech 70:867–878. https://doi.org/10.1007/s00466-022-02212-8
21. Zohdi TI (2022) A digital-twin and machine-learning framework for precise heat and energy management of data-centers. Comput Mech 69:1501–1516. https://doi.org/10.1007/s00466-022-02152-3
22. Zohdi T (2020) A machine-learning framework for rapid adaptive digital-twin based fire-propagation simulation in complex environments. Comput Methods Appl Mech Eng 363:112907. https://doi.org/10.1016/j.cma.2020.112907
23. Zohdi TI (2020) Modeling and simulation of the infection zone from a cough. Comput Mech 66:1025–1034. https://doi.org/10.1007/s00466-020-01875-5
24. Singh M, Srivastava R, Fuenmayor E, Kuts V, Qiao Y, Murray N, Devine D (2022) Applications of digital twin across industries: a review. Appl Sci 12:5727. https://doi.org/10.3390/app12115727
25. Pylianidis C, Osinga S, Athanasiadis IN (2021) Introducing digital twins to agriculture. Comput Electronics Agric 184:105942. https://doi.org/10.1016/j.compag.2020.105942
26. Goodrich P, Betancourt O, Arias AC, Zohdi T (2023) Placement and drone flight path mapping of agricultural soil sensors using machine learning. Comput Electronics Agric 205:107591. https://doi.org/10.1016/j.compag.2022.107591
27. Randolph O, Asiabanpour B (2020) Energy consumption optimization in off-grid vertical farming. In: Proceedings of the IIE annual conference, pp 861–866
28. Sambor D, Wilber M, Whitney E, Jacobson M (2020) Development of a tool for optimizing solar and battery storage for container farming in a remote arctic microgrid. Energies 13:5143. https://doi.org/10.3390/en13195143
29. Natarajan G, Zaid M, Konka H, Srinivasan R, Ramanathan S S, Ahmed T, Chowdhury H, (2022) Modeling of air distribution inside a shipping container plant factory using computational fluid dynamics (cfd), p 020091. https://doi.org/10.1063/5.0117095